Gas bubble motion artifact reduction through simultaneous motion estimation and image reconstruction

Kai Wang [a], Hua-Chieh Shao [a], You Zhang [a], Chunjoo Park [a], Steve Jiang [a], Jing Wang*[a]

[a]Department of Radiation Oncology, University of Texas Southwestern Medical Center, Dallas, TX 75390

ABSTRACT

Motion of gas bubbles (gastrointestinal gas) in abdominal region can produce significant artifacts during on-board CBCT scanning, which adversely affects the imaging quality and limits the process of CBCT-based adaptive planning and image-guided radiotherapy. In this study, we tested the effectiveness of simultaneous motion estimation and image reconstruction technique (SMRIE) for improving CBCT image quality and HU accuracy of abdominal scan. The improved image quality in the simulation study demonstrated that SMRIE technique is promising for on-board CBCT gas bubble motion artifact reduction.

Keywords: CBCT image reconstruction, motion artifact reduction, motion estimation

1. INTRODUCTION

Begin the Introduction two lines below the Keywords. The manuscript should not have headers, footers, or page numbers. It should be in a one-column format. References are often noted in the text[1] and cited at the end of the paper. N-board cone-beam computed tomography (CBCT) is widely used in image-guided radiation therapy (IGRT) and shows the potential to aid in adaptive radiation therapy (ART)[1-4]. Its artifacts, range from those due to inherent limitation of imaging physics, such as scattering, beam hardening, to those caused by the long-time scanning process, such as patient respiratory motion, have been well studied [5-7]. Much work has been done on techniques to reduce these artifacts and improve the imaging quality. However, the artifacts produced by isolated aperiodic motions of small structures, such as gastrointestinal gas bubble, have been rarely described, and no available method has been discussed to correct them to our knowledge [2,4]. As the gas bubble motion artifact is frequently seen in abdominal scan and could induce severe artifacts (as shown in Fig. 1), an artifact correction method designed for gas bubble motion is desired to improve the abdominal CBCT image quality and then aid in online patient setup and adaptive radiation therapy. Serval studies have been conducted to characterize the imaging features of gas bubble motion artifacts through phantom and/or clinical experiment [6,8,9]. These studies revealed that data inconsistency of the high-contrast tissue-air boundary on different x-ray projections due to gastrointestinal peristalsis is the main reason for the streaky and/or hyperdense artifacts, and the shape of artifact can be affected by the size, speed, position and moving direction of gas bubble. Through viewing the patient scans, they found small intestine area was the most commonly affected region.

Winklhoder *et al*. used rapid-kV switching (rs) dual-energy computed tomography (DECT) to reduced gastrointestinal peristalsis-related steak artifact and observed significant artifact reduction in both phantom and patient abdominal imaging [7]. However, the current on-board CBCT doesn't have energy discrimination ability, and the required time for scanning of on-board CBCT is much longer than diagnostic CT which could induce more gas bubble motion artifacts. Liu *et al*. proposed a cycle generative adversarial network (cycleGAN) for post-imaging processing of on-board abdominal CBCT and generate high-quality CBCT-based synthetic CT (sCT) for pancreatic adaptive radiotherapy [4]. Although much less gas bubble artifact can be seen in the generated sCT, the post-processing strategy and black-box property of deep learning might lead to fake abdominal structures in the regions affected by artifacts.

*Jing.Wang@UTSouthwestern.com; phone 214-648-1795

Figure 1. On-board abdominal CBCT gas bubble artifacts in different regions of a same patient in a single scan (-300~300 HU).

As the distribution and motion of gas bubbles in abdominal region are irregular in temporal domain, the widely used phase partition strategy for 4D CBCT motion artifact reduction cannot be readily applied for gas bubble artifact reduction. To overcome this limitation, we hypothesize that if the CBCT projection images were continuously divided into small groups, the gas bubble motion within each group can be neglected, an artifact reduced image can be reconstructed through estimation of the deformation vector fields (DVFs) between each group in image domain and motion-compensated image reconstruction.

Based on this hypothesis, in this work, we utilize the simultaneous motion estimation and image reconstruction (SMEIR) approach for abdominal CBCT image reconstruction and obtain the motion vectors simultaneously. The performance of the proposed strategy was evaluated with a simulation study.

2. MATERIALS AND METHODS

2.1 The SMEIR algorithm

SMEIR algorithm has two main steps: motion estimation and motion-compensated reconstruction. Before SMEIR, we reconstructed an initial reference image using all the current projection images with simultaneous algebraic reconstruction (SART) method. Because of the existence of gas bubble motion during CBCT scan, the initial image would contain gas bubble motion artifacts, similar to images in Fig. 1. Different from the original SMEIR which was proposed for respiration artifact reduction, there is no motion phase information to guide motion phase partition for gas bubble motion. Instead, we evenly divided the projections into N projection groups following our hypothesis, each group has continued projection images covering $360°/N$ projection angle. We then applied the Demons registration algorithm to generate the initial inter-group DVFs between the reference group (group 1 in our experiment) and all other groups. 2D projection images from each projection group and 3D reference reconstruction image were used here for the corresponding DVF estimation. In the motion-compensated reconstruction step, we used all the projection images and the estimated DVFs to reconstruct a new reference CBCT by using the motion-compensated simultaneous algebraic reconstruction method (MC-SART). These two steps were iteratively used until the reconstruction process reached the converge condition. The overall workflow of SMEIR method for abdominal CBCT gas bubble motion artifact reduction is shown in Fig. 2, and the objective function is:

$$\widehat{\mu^1}, \hat{v} = \underset{\mu^1, v}{\operatorname{argmin}} \sum_{n=1}^{N} \|p^n - A\mu^1(x + v^{1 \to n})\| + \beta\phi_1(\mu^1) + r\phi_2(v) \tag{1}$$

where μ^1 is the line attenuation coefficient of CBCT at group 1, $v^{1 \to n}$ denotes the deformation matrix to transform CBCT from group 1 to group n (n=1, 2, …, N), p is the projection, β and r are regularization terms which control the balance between data fidelity, image total variation sparsity and DVF smoothness constrain. A is the CBCT projection system matrix, which was calculated through ray-tracing technique. Regularization function ϕ_1 is total variation in our study, and ϕ_2 measures free-form energy of the deformation fields which is defined as:

$$\phi_2(v) = \sum_{v \in R^3} \sum_{i=1}^{3} \sum_{j=1}^{3} \left(\frac{\partial v^i}{\partial x^j}\right)^2 \tag{2}$$

To be specific, in the 2D-3D registration motion estimation step, we iteratively update the following objective functions group by group:

$$\hat{v}^{n \to 1} = \underset{v^{n \to 1}}{\operatorname{argmin}} \|p^1 - A\mu^n(x + v^{n \to 1})\| + r\phi_2(v^{n \to 1}) \tag{3}$$

$$\hat{v}^{1 \to n} = \underset{v^{1 \to n}}{\operatorname{argmin}} \|p^n - A\mu^1(x + v^{1 \to n})\| + r\phi_2(v^{1 \to n}) \tag{4}$$
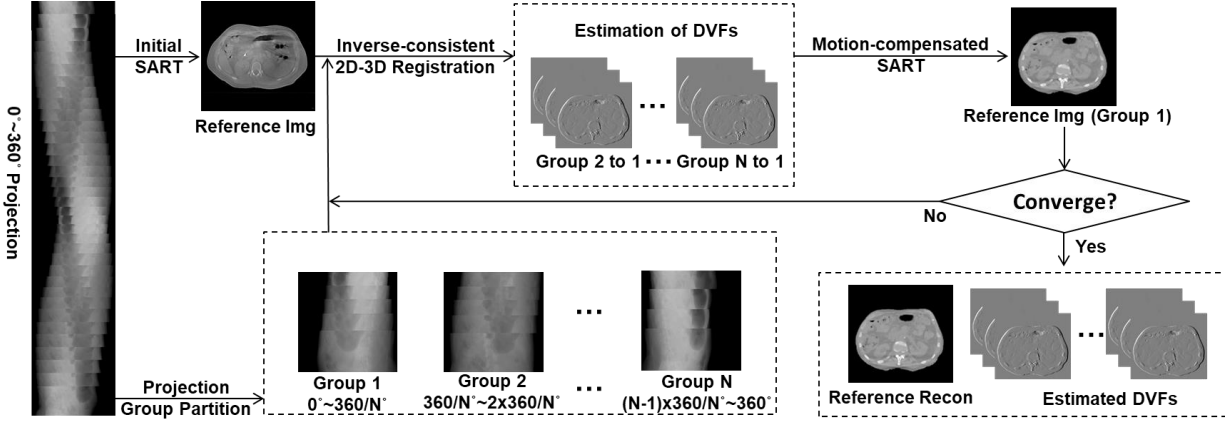
Figure 2. Workflow of gas bubble artifact reduction using simultaneous motion estimation and image reconstruction (SMEIR) method. SART: simultaneous algebraic reconstruction technique; DVF: deformation vector field; N: number of projection groups.

r is empirically set to 0.05 in our study. Nonlinear conjugate gradient algorithm was used to minimize these two functions alternatively, the DVFs updated in the first function were inverted and served as the initial for the second function. T_1=5 iterations were used in our experiment for motion estimation in each iteration of SMEIR.

In MC-SART step, we have the current reconstruction results for each group as:

$$\mu^n = \mu^1(x + v^{1\to n}) \tag{5}$$

and the reference group image can be updated through a modified SART algorithm, which is:

$$\mu_j^{1,new} = \mu_j^1 + \lambda \frac{\sum_{n,k} d_{jk}^{n\to 1} \sum_i [a_{ik} \frac{p_i - \sum_k a_{ik} u_k^n}{\sum_{k=1}^J a_{ik}}]}{\sum_{n,k} d_{jk}^{n\to 1} \sum_i a_{ik}} \tag{6}$$

where $d_{jk}^{n\to 1}$ denotes element of the DVF matrix that deforms image from group n to group 1. T_2=10 iterations were used in our study for motion compensated reconstruction in each iteration of SMEIR.

2.2 Material

To simulate the irregular motion during on-board CBCT scanning, we used two 3D abdominal CT images for a same patient acquired with 3 mins interval as the base images in this study. Dimension of the CT images are both 512×512×256, with voxel size of 0.125×0.125×0.192cm³. The deformation vector field (DVF) between these two scans were calculated in the image domain and used as $v^{1\to N}$, and other N-2 (N=4, 8, 16) different DVFs were generated through randomly scaling $v^{1\to N}$ in x, y, z directions by [-2, 2] to the simulate different DVFs. Then, the first CT image was deformed to $N-2$ different CT images corresponding to the simulated DVFs. A N group 360° full-fan CBCT projection was then simulated through combining the projection images from different CT images, where projections from every continuous 360°/N beam angle are generated from the same CT image using the ray tracing technique. The total number of projection images are set as 360, detector size is 1280×318 with pixel size 0.0772×0.1344cm², SP. To explore the effect of selection of group number N, N=4, 8, 16 were simulated in our experiment. For image reconstruction, image dimension of 256×256×128 with voxel size of 0.25×0.25×0.25cm³ were used, and we ran 20 iteration of SMEIR for all the experiments.

3. RESULTS

We showed the original group 1 image sample slices and reconstructed image with different methods and motion groups in Fig. 3. The real gas bubble artifacts in an on-board CBCT abdominal scan are shown in Fig. 1, while the simulated gas bubble artifacts in 4-, 8- and 16-groups simulated CBCT scan with SART reconstruction are shown in Fig. 3 (b)~(d). As the simulated motion mainly occurred on a single large air bubble (stomach) the pattern of artifacts in these images are more similar to the third image in Fig. 1. The corresponding reconstructed image with SMEIR is shown in Fig. 3 (e)~(g).
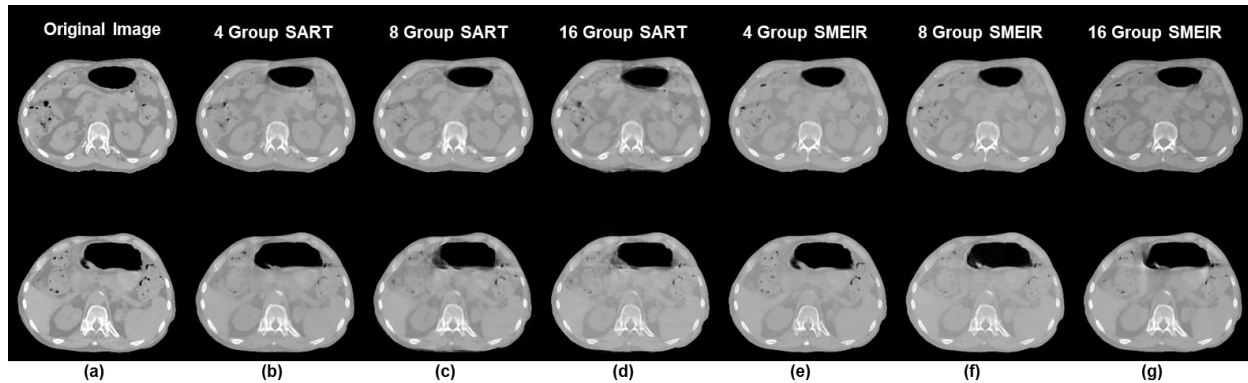
Figure 3. Original group 1 images, simulated gas bubble artifacts in SART results, and reconstructed images with SMEIR. (a) are two slices of original group 1 image. (b)~(d) are the SART reconstruction of different motion group projections, simulated gas bubble motion artifacts can be seen around the boundary of the gas bubble in the images. (e)~(g) are the SMEIR results which reduced the artifact around the gas bubble boundaries.

As the number of motion groups increase, in the SART reconstructed images, the visual quality of the gas bubble boundary became more blurred, and small streak artifact can be seen when N=16. Compared to the SART reconstruction results, the boundaries of reconstructed gas bubbles with SMEIR are well preserved and HU values around bubble regions are more accurate when compared with the original group 1 images, no obvious streak artifact can be seen.

4. DISCUSSIONS AND CONCLUSION

In this study we modified SMEIR for gas bubble motion artifact reduction. From the simulation experiment, we can clear see the image quality improvement in the gas bubble boundary area by using SMEIR over SART.

There are several limitations of the current study. First, scattering is an important factor that influences CBCT imaging quality, for a more realistic simulation, we need to consider it in a future study. Second, given the inherent irregularity of gas bubble motion in both temporal domain and spatial domain, it's difficult to simulate the gas bubble motion. Our next step will be more focusing on artifact reduction using real clinical data. Third, dividing the projection data into projection groups equally is not an optimal strategy. The larger the N is, the smaller the motion within each projection group, and smaller angle coverage. Although big N can improve the data consistency within each projection group, small projection angle coverage might not provide enough information to update the DVF. Therefore, a data-driven projection group partition method is desired.

Deep learning-based methods have showed promising performance on both medical image reconstruction and post-processing tasks, and serval cycleGAN-style networks were proposed to synthesis high-quality images using CBCT for CBCT-guided adaptive radiotherapy [4, 10]. Although not designed for gas bubble motion artifact reduction, some of them performed well in the abdominal region [4]. One of our future works will be incorporating deep learning methods to the workflow of gas bubble motion artifact reduction and motion estimation.

In conclusion, we introduced SMRIE technique for gas bubble motion artifact reduction, the improved image quality of the gas bubble area in this study demonstrated that SMRIE technique is promising for on-board CBCT gas bubble motion artifact reduction.

REFERENCES

[1] Ding GX, Duggan DM, Coffey CW, et al. A study on adaptive IMRT treatment planning using kV cone-beam CT. Radiotherapy and Oncology. 2007;85(1):116-125.
[2] Wang J, Gu X. Simultaneous motion estimation and image reconstruction (SMEIR) for 4D cone-beam CT. Medical physics. 2013;40(10):101912.

[3] Li Y, Hoisak JD, Li N, et al. Dosimetric benefit of adaptive re-planning in pancreatic cancer stereotactic body radiotherapy. Medical Dosimetry. 2015;40(4):318-324.

[4] Liu Y, Lei Y, Wang T, et al. CBCT-based synthetic CT generation using deep-attention cycleGAN for pancreatic adaptive radiotherapy. Medical physics. 2020;47(6):2472-2483.

[5] Estabrook NC, Corn JB, Ewing MM, Cardenes HR, Das IJ. Dosimetric impact of gastrointestinal air column in radiation treatment of pancreatic cancer. The British journal of radiology. 2017;91(xxxx):20170512.

[6] Lee JS, Kim SH, Kim JJ, Kim BS, Choi GM, Kim DR. Gastrointestinal Air Motion Artifact Which Can Be Mistaken for Active Gastrointestinal Bleeding in Multidetector Computed Tomography: Phantom and Clinical Study. Journal of computer assisted tomography. 2020;44(1):145-152.

[7] Winklhofer S, Lambert JW, Wang ZJ, et al. Reduction of peristalsis-related gastrointestinal streak artifacts with dual-energy CT: a patient and phantom study. Abdominal radiology. 2016;41(8):1456-1465.

[8] Liu F, Cuevas C, Moss AA, Kolokythas O, Dubinsky TJ, Kinahan PE. Gas bubble motion artifact in MDCT. American Journal of Roentgenology. 2008;190(2):294-299.

[9] Clackdoyle R, Desbat L. Data consistency conditions for truncated fanbeam and parallel projections. Medical physics. 2015;42(2):831-845.